doi:10.1093/brain/awr300 Brain 2011: 134; 3694–3704 | 3694

BRAIN
A JOURNAL OF NEUROLOGY

Cerebrovascular lesions induce transient β-amyloid deposition

Monica Garcia-Alloza,[1,2] Julia Gregory,[1] Kishore V. Kuchibhotla,[1] Sara Fine,[1] Ying Wei,[3] Cenk Ayata,[3,4] Matthew P. Frosch,[1,5] Steven M. Greenberg[1] and Brian J. Bacskai[1]

1 Alzheimer Research Unit, Department of Neurology, Massachusetts General Hospital and Harvard Medical School, 114 16th Street, Charlestown, MA 02129, USA
2 Division of Physiology, School of Medicine, University of Cádiz, Plaza Fragela, s/n planta 4a, Cádiz 11003, Spain
3 Stroke and Neurovascular Regulation Lab, Department of Radiology, Massachusetts General Hospital, 149 13th Street, Charlestown, MA 02129, USA
4 Stroke Service and Neuroscience, Intensive Care Unit, Department of Neurology, Massachusetts General Hospital, 149 13th Street, Charlestown, MA 02129, USA
5 C.S. Kubik Laboratory for Neuropathology, Department of Pathology, Massachusetts General Hospital and Harvard Medical School, 55 Fruit Street, Boston, MA 02114, USA

Correspondence to: Brian J. Bacskai, PhD,
Massachusetts General Hospital,
Department of Neurology/Alzheimer's Disease Research Laboratory,
114 16th Street, #2010,
Charlestown, MA 02129, USA
E-mail: bbacskai@partners.org

Previous clinical studies have documented a close relationship between cerebrovascular disease and risk of Alzheimer's disease. We examined possible mechanistic interactions through use of experimental stroke models in a transgenic mouse model of β-amyloid deposition (APPswe/PS1dE9). Following middle cerebral artery occlusion, we observed a rapid increase in amyloid plaque burden in the region surrounding the infarction. In human tissue samples, however, we were unable to detect a localized increase in amyloid burden adjacent to cerebral infarcts. To resolve this discrepancy, we generated cerebral microstrokes in amyloid precursor protein mouse models with the photosensitive dye Rose bengal, and monitored plaque formation in real time using multiphoton microscopy. We observed a striking increase in the number of new plaques and amyloid angiopathy in the area immediately surrounding the infarcted area; however, the effect was transient, potentially resolving the discord between mouse and human tissue. We did not detect changes in candidate proteins related to β-amyloid generation or degradation such as β-amyloid-converting enzyme, amyloid precursor protein, presenilin 1, neprylisin or insulin-degrading enzyme. Together, these results demonstrate that strokes can trigger accelerated amyloid deposition, most likely through interference with amyloid clearance pathways. Additionally, this study indicates that focal ischaemia provides an experimental paradigm in which to study the mechanisms of plaque seeding and growth.

Keywords: Alzheimer's disease pathology; stroke; amyloid
Abbreviations: APP = amyloid precursor protein; BACE = β-amyloid-converting enzyme

Received April 26, 2011. Revised September 23, 2011. Accepted September 25, 2011

Introduction

Virtually all risk factors for vascular disease are also risks for dementia: midlife hypertension (Launer *et al*., 1995; de Leeuw *et al*., 2002; Reitz *et al*., 2007), midlife cholesterol (Kivipelto *et al*., 2002; Pappolla *et al*., 2003), diabetes (Luchsinger *et al*., 2007), hyperinsulinaemia (Luchsinger *et al*., 2004), plasma homocysteine (Seshadri *et al*., 2002), tobacco use (Ott *et al*., 1998), metabolic syndrome (Razay *et al*., 2007), and an overall composite measure of arteriosclerosis (Hofman *et al*., 1997; Honig *et al*., 2005) have each been implicated as risks for cognitive impairment. Epidemiological studies have shown that vascular factors predisposing to cerebrovascular disease or stroke are associated specifically with Alzheimer disease and that cerebrovascular disease increases the presence and severity of the clinical symptoms of Alzheimer's disease (Breteler, 1994, 2000; Ellis *et al*., 1996; Kalaria, 2000; Launer *et al*., 2008; Helzner *et al*., 2009).

At a minimum, these associations between vascular risk factors and dementia reflect the additive effects on cognitive function of vascular brain injury and amyloid-related brain injury, a major pathological hallmark of Alzheimer's disease (Hyman, 1997). Beyond that, however, it remains possible that cerebrovascular disease interacts with the β-amyloid cascade at a mechanistic level. Such a relationship might occur if cerebral ischaemia potentiated one of the steps leading to β-amyloid deposition, such as by accelerating β-amyloid production or impairing β-amyloid clearance (Stone, 2008; Hiltunen *et al*., 2009). It has been suggested that one method by which brain levels of β-amyloid are reduced (clearance along perivascular drainage pathways) may be impaired by thromboembolic occlusion of the artery feeding a particular brain territory (Yow and Weller, 2002; Weller *et al*., 2008).

We used transgenic mouse models, including APPswe/PS1dE9 and tg2576, to test the effects of cerebrovascular lesions on β-amyloid deposition in brain parenchyma in the form of senile plaques and in small superficial vessels as cerebral amyloid angiopathy. Our hypothesis was that such lesions would interfere with local clearance of β-amyloid and thereby promote deposition in the brain territory perfused by the lesioned blood vessels. We also examined human tissue samples from patients diagnosed with both Alzheimer's disease and stroke.

Materials and methods

Animals

APPswe/PS1dE9 mice (Jankowsky *et al*., 2001) aged 6–7 months old were obtained from Jackson Laboratory, and Tg2576 mice (Hsiao *et al*., 1996) aged 11–13 months were used. All studies were conducted with approval of the Massachusetts General Hospital Animal Care and Use Committee and in compliance with National Institutes of Health guidelines for the use of experimental animals.

Human tissue

All studies were performed using autopsy brain tissue collected through the Neuropathology Core of the Massachusetts Alzheimer Disease Research Centre with approval from the Partners Human Research Committee. All subjects had both a clinical and neuropathological diagnosis of Alzheimer's disease according to the accepted criteria. Paraffin embedded sections of inferior parietal lobule were examined, with four subjects having no evidence of ischaemia in this region and three with an area of remote ischaemic infarction involving a portion of the sampled cortex.

Reagents

Texas Red® dextran of 70 000 D molecular weight was obtained from Molecular Probes; methoxy-XO4 was a gift from Dr Klunk (University of Pittsburgh); Ketamine HCl and xylazine were obtained from Phoenix Pharmaceuticals, anti-β-amyloid antibody (10D5) (developed in mouse) was a gift from Elan Pharmaceuticals; anti-β-amyloid-converting enzyme (BACE) antibody (developed in rabbit) was obtained from ProSci Incorporated; anti-amyloid precursor protein (APP) antibody (developed in rabbit) was obtained from Calbiochem; anti-insulin degrading enzyme (developed in goat) was obtained from Santa Cruz; and anti-neprilysin (developed in rat) was obtained from R&D Systems. Secondary Cy-3-conjugated antibodies were obtained from Jackson Immunoresearch Laboratories Inc.; Rose bengal, anti-presenilin 1 antibody (developed in goat), thioflavin S, Mayer's haematoxylin, eosin and common chemical reagents were obtained from Sigma.

Yellow fluorescent protein expression in layer 1 dendrites of the neocortex

Yellow fluorescent protein was expressed in a subset of mice using genetic transfer via an adeno-associated virus (serotype 2). The yellow fluorescent protein was part of a larger cassette that was prepared and injected as previously described (Kuchibhotla *et al*., 2008). We used the construct pAAV-CBA-YC3.6-WPRE. The plasmid contained the AAV inverted terminal repeats, the only remaining feature of the wild-type AAV genome. Flanked by the repeats, the expression cassette included the following components in 5′–3′ order: (i) a 1.7 kb sequence containing hybrid cytomegalovirus (CMV) immediate-early enhancer/chicken β-actin promoter/exon1/intron; (ii) yellow cameleon 3.60 complementary DNA; and (iii) woodchuck hepatitis virus post-transcriptional regulatory element (WPRE). The virus titre was 1.1×10^{12} viral genomes/ml

For intracortical injections of YC3.6-AAV2, 6–7 month old APPswe/PS1dE9 mice were anaesthetized with isoflurane and placed in a custom made, heated stereotaxic apparatus. A 2–3 mm incision was made in the scalp along the midline between the ears. Burr holes were drilled in the skull, 1 mm lateral to bregma bilaterally. Using a Hamilton syringe, 4 μl of virus (titre 4.2×10^{12} viral genomes/ml) was injected 1.2-mm deep in somatosensory cortex (targeting layer 5 neurons) at a rate of 0.2 μl/min. After one injection in each burr hole, the scalp was sutured and the mouse was allowed to recover from anaesthesia on a heating pad. After a $>$ 4 week incubation period to allow expression of YC3.6 in neurons, cranial windows were implanted.

Cranial window implantation and microstroke production

APPswe/PS1dE9 mice with and without YC-AAV2 injections, and Tg2576 mice were anaesthetized and cranial windows were implanted as previously described (McLellan *et al*., 2003; Garcia-Alloza *et al*., 2010). To produce targeted strokes using photothrombosis,

Rose bengal was administered by tail vein injection (100 μl, 25 mg/kg in sterile phosphate-buffered saline) as previously described (Zhang and Murphy, 2007) with minor modifications. An Olympus Fluoview 1000MPE with pre-chirp optics and a fast acousto-optical modulator mounted on an Olympus BX61WI upright microscope and Olympus ×20 dipping objective (numerical aperture 0.95) were used to provoke the photothrombotic microstrokes and determine the velocity of red blood cells. Rose bengal was activated using 543 nm laser (100%) directed to the selected arterial segment (~20 × 20 μm) from 2 to 3 vessels, 20–50 μm in diameter, located under the right hemisphere of the cranial window. Red blood cell velocity was assessed using repeated line scans of the same area at 860 nm (×6 zoom) through the horizontal part of the selected region of interest as previously described (Zhang and Murphy, 2007). Twenty-four and 48 h after the blockage animals were anaesthetized and the blood flow was checked again in the same spots using Texas Red dextran (70 000 D), intravenous red blood cell velocity was measured as previously described (Zhang and Murphy, 2007) using ImageJ software. Vessel diameter was measured in ImageJ at three points along each vessel segment and the average diameter was taken from these three measurements.

In vivo imaging

β-Amyloid was visualized with methoxy-XO4, a Congo red derivative that binds fibrillar β-amyloid, that was injected intraperitoneally the day before each imaging session. Angiograms were performed with 12.5 mg/ml intravenous injection of Texas Red® dextran preceding each imaging session. As previously described, two-photon fluorescence was generated with 750 nm excitation and fluorescent emission was collected in the range of 380–480 nm for methoxy-XO4, and 560–650 nm for Texas Red® dextran or Rose bengal. A ×20 (0.95 numerical aperture, Olympus) water immersion objective (615 × 615 μm, z/step 5 μm, depth ~200 μm) was used on a Fluoview 1000MPE microscope (Olympus). Maximum intensity projections of *z*-series were generated using ImageJ software. Stacks were used to measure plaque size and number (Garcia-Alloza *et al*., 2010). Senile plaque size was measured by thresholding, segmenting and measuring using the blue fluorescence channel and ImageJ software. Cerebral amyloid angiopathy burden was also analysed in maximum intensity projections as previously described (Robbins *et al*., 2006; Garcia-Alloza *et al*., 2009*a*). Autofluorescent signal from the dura was removed by deleting the uppermost slices of the *z*-series. Vessels were outlined and the cerebral amyloid angiopathy deposits, appearing as bright areas circumferential to the vessels, were manually thresholded so that cerebral amyloid angiopathy-positive regions were set white and cerebral amyloid angiopathy-negative regions were set black. The number of pixels in white clusters composed of >6 contiguous pixels was counted. The cerebral amyloid angiopathy burden was calculated as the percentage of the vessel area affected by cerebral amyloid angiopathy. The vessel area from the initial imaging session was used for calculation of cerebral amyloid angiopathy burden because of the tendency for vessels to dilate in subsequent weeks. New growth of cerebral amyloid angiopathy deposits was measured from week to week. Vessel diameter was measured in ImageJ at three points along each vessel segment and the average diameter was taken from these three measurements. In a subset of experiments, yellow fluorescent protein-filled dendrites were imaged alongside plaque deposition to confirm the impact of photothrombotic lesions on nearby neuronal structure.

Focal cerebral ischaemia

Middle cerebral artery occlusions were performed in APPswe/PS1dE9 and age-matched non-transgenic littermates as previously described (Shin *et al*., 2008) with minor modifications. Animals were anaesthetized with isoflurane, placed in a stereotaxic frame (David Kopf) and allowed to stabilize for 30 min after preparation. The temporalis muscle was separated from the temporal bone and removed. A burr hole (2-mm diameter) was drilled under saline cooling in the temporal bone overlying the middle cerebral artery just above the zygomatic arch. The dura was kept intact and distal middle cerebral artery was occluded for 1 h using a microvascular clip. Mice were allowed to recover, and were sacrificed 7 days later. Mice were perfused with 4% paraformaldehyde. Whole brains were paraffin embedded and cut in 16 μm coronal sections.

Haematoxylin–eosin staining

Standard haematoxylin–eosin staining was performed in 1 in every 10 sections (16 μm) from APPswe/PS1dE9 mice in order to identify the stroke areas after middle cerebral artery occlusion in APPswe/PS1dE mice as well as in human tissue (6 μm) to identify stroke areas in tissue from patients with Alzheimer's disease. Tissue was deparaffinized and incubated for 8 min in Mayer's haematoxylin solution and washed in warm water for 10 min. Sections were dipped in 95% ethanol and counterstained with eosin for 30 s.

Thioflavin S staining and plaque counting

Senile plaque size was measured in post-mortem tissue in the stroke areas from APPswe/PS1dE9 mice after middle cerebral artery occlusion. Stroke areas were delimited by haematoxylin–eosin staining and the selected area in the ipsilateral hemisphere was used as a phantom area in the contralateral hemisphere for comparison. One in every 10 sections from stroke areas was stained with thioflavin S (0.1%) for 20 mins and carefully rinsed in water before mounting an aqueous coverslip. Micrographs of stained tissue were obtained on an upright Olympus BX51 fluorescence microscope with a DP70 camera using DPController and CPManager software (Olympus). Senile plaque size was measured by thresholding, segmenting and measuring using the blue fluorescence channel and ImageJ software. Similarly, in human tissue from patients with Alzheimer's disease, stroke areas were delimited by haematoxylin–eosin staining. Thioflavin S staining was used to plot plaque number versus distance to the stroke area, in order to assess a possible gradient effect of the strokes on senile plaque deposition up to 2000 μm from the stroke area boundaries. Selected areas in tissue from patients with Alzheimer's disease with strokes were used as phantoms in non-stroke Alzheimer's disease tissue as control, and the number of plaques as a function of distance was also plotted.

Immunohistochemistry

Immunohistochemistry with anti-β-amyloid, anti-BACE, anti-presenilin 1, anti-neprilysin and anti-insulin degrading enzyme antibodies was performed in tissue from APPswe/PS1dE9 mice after middle cerebral artery occlusion. Briefly, tissue was deparaffinized and sections were washed in Tris-buffered saline for 30 mins, blocked with normal goat serum (5%) for 1 h and incubated overnight at 4°C with primary antibodies [1:50 for anti-Aβ (10D5) and anti-BACE antibodies, and

1:100 for anti-presenilin 1, anti-APP and anti-insulin degrading enzyme antibodies and 1:20 for anti-neprilysin]. After washing in Tris-buffered saline, sections were incubated in conjugated Cy-3 secondary antibodies (1:100–200) for 1 h, rinsed and aqueously coverslipped.

Results

Senile plaque deposition is increased after middle cerebral artery occlusion

In order to evaluate the relationship between focal ischaemia and amyloid deposition characteristic of Alzheimer's disease, we performed transient unilateral middle cerebral artery occlusion in APPswe:PS1dE9 mice at an age where amyloid plaque deposition was detectable. The animals survived the insults, and were sacrificed 1 week later. The brains of the animals were probed for amyloid deposits with histo- and immunohistological approaches in coronal sections of post-mortem tissue. Adjacent sections were processed with haematoxylin and eosin following standard protocols to allow delineation of the stroke volume within the brain. Although variable, stroke volumes showed a tendency to be enlarged in transgenic mice when compared with wild-type animals (~9.80 versus ~4.56 mm^3, Student *t*-test for independent samples, $P = 0.086$) as has been previously described in other APP mouse models (Zhang *et al.*, 1997; Koistinaho *et al.*, 2002). Fig. 1 shows an example of haematoxylin–eosin staining, and thioflavin S staining in the middle cerebral artery occlusion territory of the lesioned hemisphere, and the contralateral territory of the same mouse, which was used as a control for the variability in plaque density between APP mice of the same age. There were significantly more senile plaques detected in the ipsilateral versus contralateral hemisphere and media (minimum–maximum) were as follows [83 (28–156) versus 75 (74–123)/mm^2, $^{**}P < 0.009$ Wilcoxon test for paired samples, four mice, 4–5 sections per mice]. The average size of the plaques was not significantly different between hemispheres (223 ± 10 versus $199 \pm 9\,\mu m^2$, $P = 0.08$, $n = 961$–1233 plaques from four mice, 4–5 sections per mice). To test whether the increased plaque deposition was restricted to dense-core versus diffuse amyloid aggregates, we used 10D5, an N-terminal specific anti-β-amyloid antibody for immunostaining in adjacent sections from the same mice. We found complete co-localization of immunostaining with thioflavin S staining suggesting that the rapid appearance of dense core plaques was not associated with diffuse amyloid plaques (data not shown).

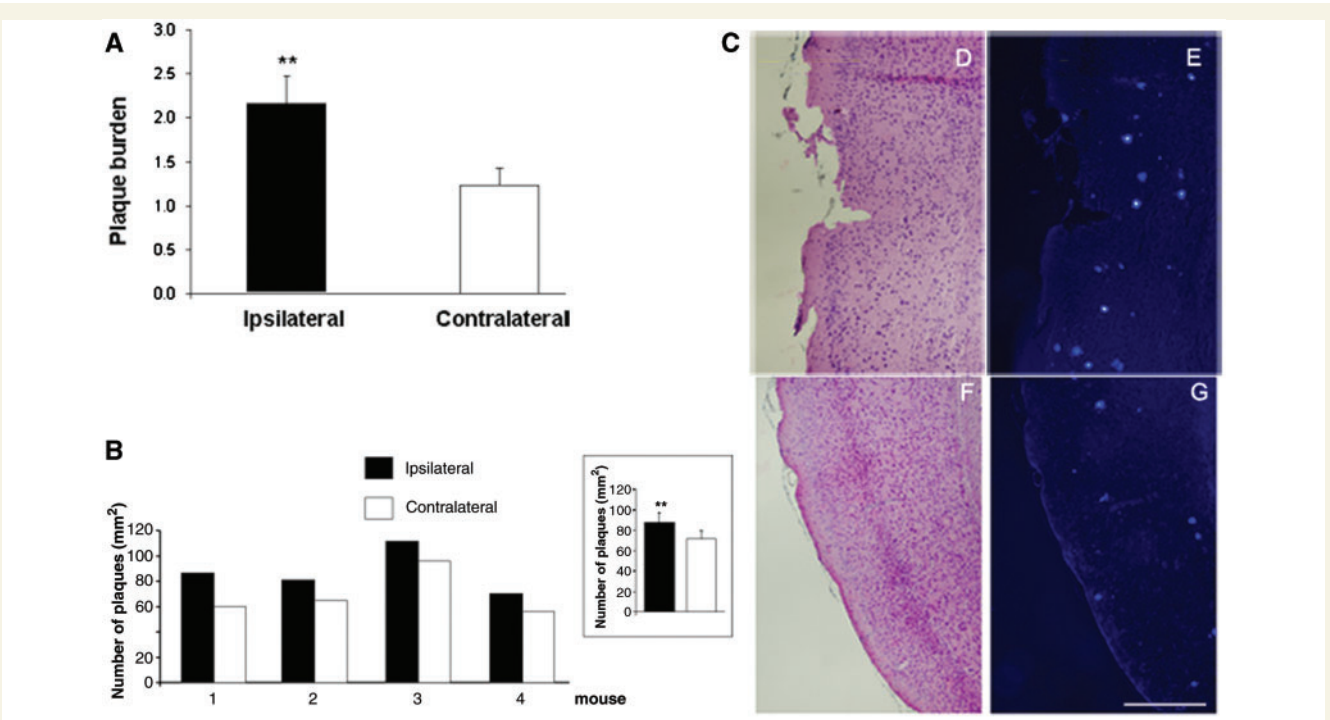

Figure 1 (**A**) Increased plaque burden is observed in cortex 7 days after middle cerebral artery occlusion in APPswe/PS1dE9 mice. Brain sections were stained with haematoxylin–eosin in order to identify stroke regions and 1 every 10 sections in the stroke area was analysed using thioflavin S staining. Data are representative of five animals. Differences in plaque burden were detected by Student *t*-test for paired samples ($^{**}P = 0.001$ versus contralateral cortex). (**B**) Comparison between ipsilateral and contralateral plaque number per millimetre square in the four animals under study. An overall difference is observed using Wilcoxon for paired samples (inlet $^{**}P = 0.009$). (**C**) Representative example of haematoxylin–eosin staining in ipsilateral (**D**) and contralateral (**F**) stroke regions 7 days after middle cerebral artery occlusion. Cortical layer distribution is preserved in contralateral versus ipsilateral hemispheres. Thioflavin S staining shows increased amyloid deposition in the stroke areas (**E**) when compared with contralateral regions (**G**). Scale bar = 500 μm.

Effect of stroke on senile plaque deposition in patients with Alzheimer's disease

The ability to detect increased amyloid burden within the ischaemic territory of experimental stroke in the animal model motivated us to examine human tissue in a complementary fashion. We obtained samples of post-mortem human tissue with a diagnosis of both Alzheimer's disease and moderate stroke. Using haematoxylin–eosin staining to delineate the stroke volumes, we probed for amyloid deposition with thioflavin S, and compared the amyloid burden in the areas of the brain immediately adjacent to the lesion. The regular distribution of the plaques was not affected by strokes up to 2000 μm from the stroke volumes as shown in Fig. 2. The data also indicate that no differences in plaque size were observed in the surround of the stroke areas when compared with non-stroke patients (235 ± 7 versus 251 ± 5 μm^2, n = 627–1444 from 3 to 4 patients).

The lack of a detectable difference in β-amyloid burden surrounding stroke volumes in human tissue is consistent with literature reports, but surprising in the context of our experiments eliciting strokes in experimental animals. We postulated that the discrepancy could be related to the duration of a stroke-mediated effect on amyloid deposition, prompting us to examine the kinetics of the interaction between ischaemia and β-amyloid deposition.

Photothrombosis-mediated ischaemia increases β-amyloid deposition locally

To examine the timing of β-amyloid deposition following ischaemic stroke, we made longitudinal measurements of amyloid burden using multiphoton microscopy and systemic labelling of amyloid deposits with methoxy-XO4 as we have done previously (Garcia-Alloza *et al*., 2009*a*,*b*, 2010). In tandem, we generated ischaemic lesions by eliciting photothrombosis using Rose bengal as a photosensitizing agent within individual vessels as previously described (Zhang and Murphy, 2007). This approach allows targeting a single vessel to study thrombosis and β-amyloid deposition in a time-dependent manner. The efficacy of induction of ischaemia was examined by measuring the instantaneous velocity of red blood cells in affected and nearby vessels. This allowed us to demonstrate that the photothrombosis method resulted in complete cessation of blood flow in the targeted vessel that lasted 1–2 days, and substantial alterations in blood flow in the immediate surround of the occlusion (data not shown). Severe morphological changes to neurites in the affected areas were detected with

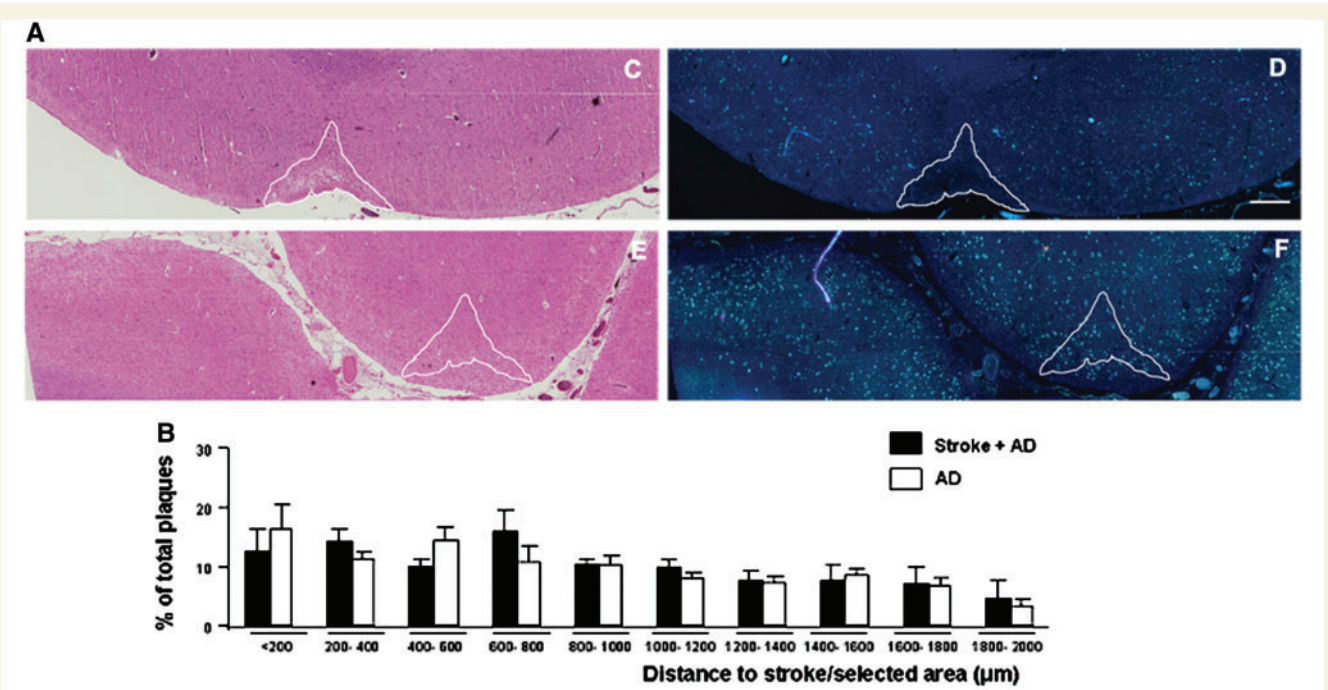

Figure 2 (**A**) Stroke areas in human tissue are not associated with increased amyloid burden. Representative example of human cortical tissue from Alzheimer's disease-stroke patient (**C**: haematoxylin–eosin, **D**: thioflavin S) and from a patient with Alzheimer's disease (**E**: haematoxylin–eosin, **F**: thioflavin S). The stroke area was identified and outlined in the haematoxylin–eosin stained section and the same outline was used to count plaques and distance to the stroke area with thioflavin S. Same selection was made in Alzheimer's disease tissue to count plaques and measure distance to phantom stroke area. Scale bar = 500 μm. (**B**) Number of plaques counted in the cortex and distance to the stroke area are represented in a histogram plotting the percentage of total plaques every 200 μm. A similar distribution of plaques is observed up to 2000 μm from the stroke area both in Alzheimer's disease-stroke tissue and Alzheimer's disease tissue. Data are representative of three Alzheimer's disease-stroke patients and four patients with Alzheimer's disease (n = 627–1444 plaques) and no differences were detected by Student t-test for independent samples ($P > 0.05$ in all subsets). AD = Alzheimer's disease.

yellow fluorescent protein-expressing neurons, as described previously (Zhang and Murphy, 2007) and shown in Fig. 3. This allowed us to define the affected volume from the point of photothrombosis as having a radius around the occluded vessel of ~250 μm (a 'microstroke'). Thus, this single vessel photothrombosis approach allowed focal ischaemic lesions in targeted areas that were readily imaged both acutely and longitudinally with multiphoton microscopy.

We imaged amyloid deposits at weekly intervals in the area of the brain with occlusions, and in adjacent areas within the same mouse where blood flow was unperturbed. We detected the appearance of many new plaques within the volume of the microstroke after 7 days [expressed as media (minimum–maximum), stroke regions 13 (0–79) versus non-stroke regions 0 (0–52)/mm^3 *P = 0.040 Mann–Whitney test for independent samples, 24–53 fields from 11 to 15 mice; Fig. 4]. At 14 days, there was no difference in the number of new plaques in the stroke volume versus the adjacent area compared with the previous week [stroke regions 7 (0–13) versus non-stroke regions 0 (0–39)/mm^2 P = 0.327 Mann–Whitney test for independent samples, 14–42 fields from 11 to 15 mice]. No differences were observed in non-stroke regions between Days 7 and 14. (Wilcoxon for paired samples P = 0.877). Importantly, the appearance of new plaques was also observed in another transgenic mouse model (Tg2576) demonstrating the broader significance of the observation. Seven days after the microstroke,

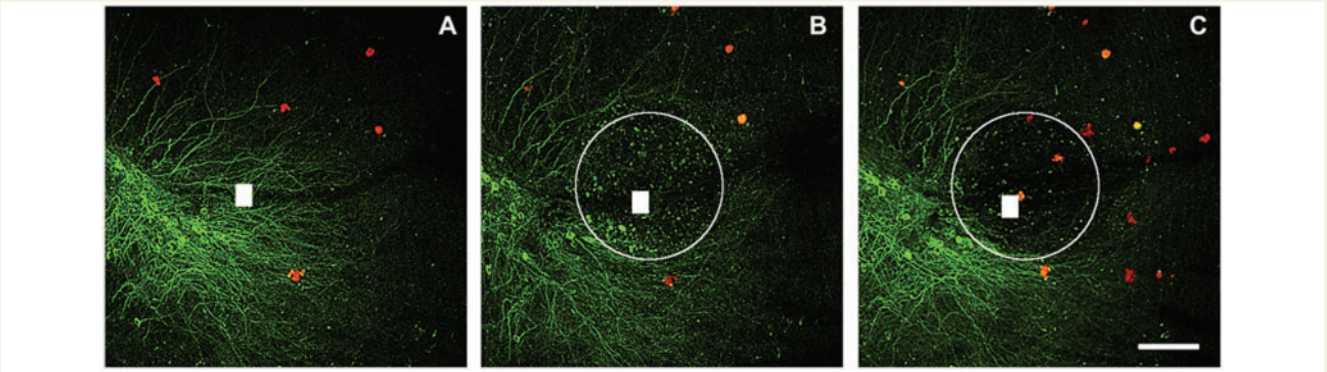

Figure 3 Microstrokes lead to the generation of new plaques. The images show yellow fluorescent protein expressing neurons in the cortex (green) along with methoxy-XO4 labelled plaques (red) before Rose bengal is used to induce a photothrombotic microstroke (**A**). Morphological disturbances of the surrounding neurites were observed as soon as 6 h after the stroke up to ~250 μm from the stroke vessel (circled area) (**B**). One week later, morphological disturbances were still present and new senile plaques were observed (**C**). The position of the occluded vessel is marked with white squares. Scale bar = 100 μm.

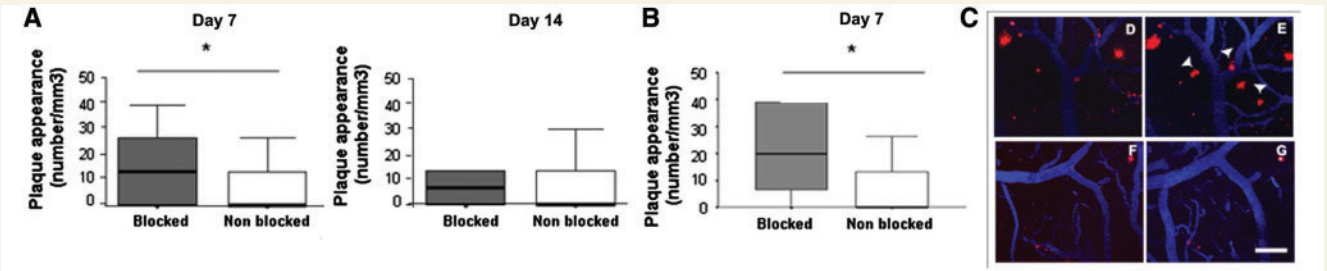

Figure 4 The increased accumulation of new plaques around microstrokes in APP mice is a transient effect. (**A**) Number of plaques appearing per cubic millimetre after 7 and 14 days of single vessel occlusion with Rose bengal. Twenty-four fields corresponding to areas containing 24 blocked vessels and 53 fields corresponding to areas not blocked or from non-treated mice at the beginning of the experiment (no differences were observed between areas not blocked or untreated mice: Mann–Whitney U test P = 0.853). Data shown represent media (maximum and minimum) from 11 to 15 mice and statistical differences were observed between both groups using Mann–Whitney U test for independent samples *P = 0.040 for Day 7, whereas no differences were observed on Day 14 (P = 0.717). (**B**) Similar differences in plaque deposition were observed in Tg2576 mice 7 days after vessel blockage. Data shown represent media (maximum and minimum) from five mice and statistical differences were observed between both groups using Mann–Whitney U test for independent samples *P = 0.048 for Day 7. (**C**) Illustrative example of the senile plaque deposition rate in APPswe/PS1dE9 mice 7 days after Rose bengal blockage of a vessel (**D**: Day 0, **E**: Day 7) compared with an area without vessel blockage (**F**: Day 0, **G**: Day 7). The same fields were located using Texas Red® dextran 70 000 D (blue) for the angiograms and amyloid deposits were stained with methoxy-XO4 (red). White squares mark the blocked area and arrows point at new amyloid deposits. Scale bar = 100 μm.

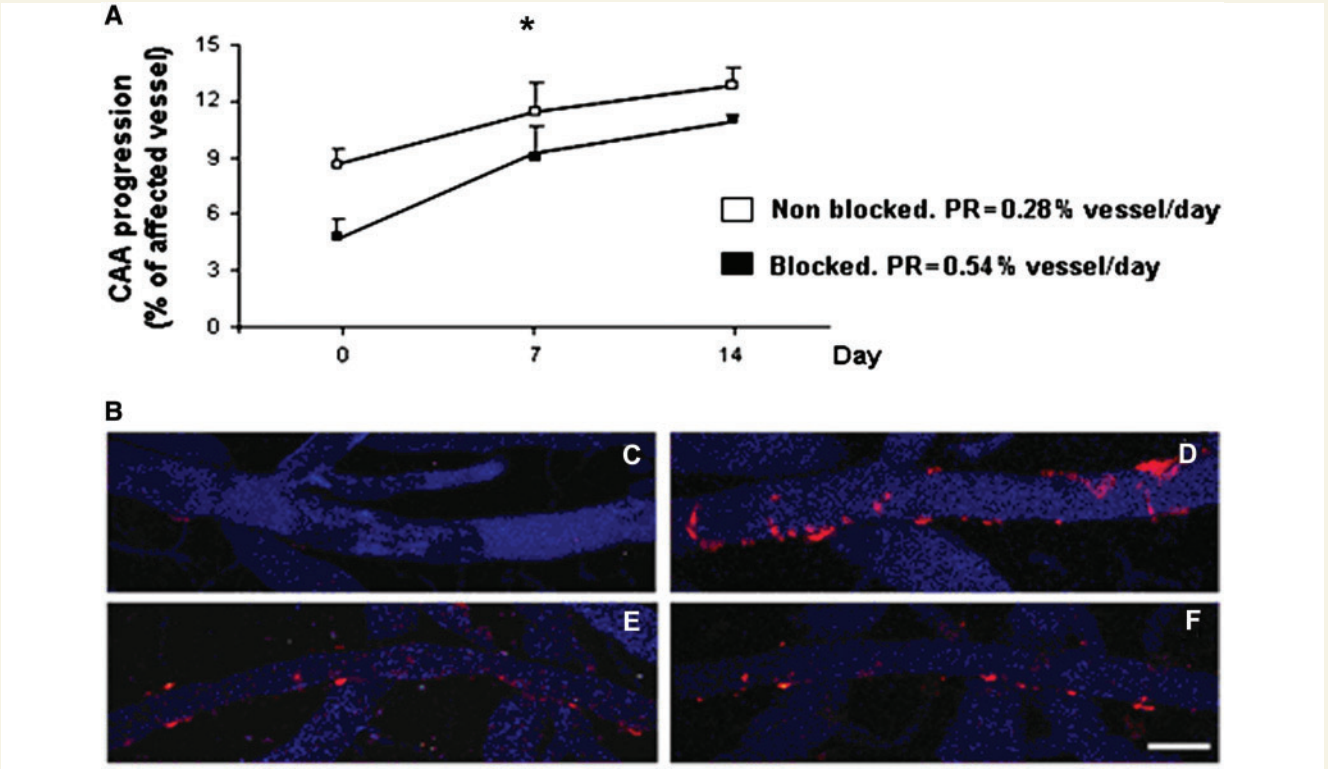

Figure 5 (**A**) Progression of cerebral amyloid angiopathy is increased in occluded vessels. Longitudinal imaging of identified vessels before single vessel occlusion as well as 7 and 14 days after the blockage in APPswe/PS1dE9 mice. Cerebral amyloid angiopathy (CAA) progression in vessels blocked using Rose bengal versus non-occluded vessels. Vessels from non-blocked mice and vessels from control mice were pooled since no differences were detected between both groups ($P = 0.649$). However, we detected a statistically significant acceleration of the cerebral amyloid angiopathy progression rate in vessels blocked with Rose bengal (progression rate = 0.54) when compared with non-blocked vessels (progression rate = 0.28) (*$P = 0.016$). (**B**) Example of cerebral amyloid angiopathy progression in a blocked vessel on Day 0 and on Day 7 (**C** and **D**) and a non-blocked vessel on Day 0 and on Day 7 (**E** and **F**). Scale bar = 25 μm.

we measured 26 (0–39)/mm^3 new plaques in stroke regions versus 0 (0–26)/mm^3 new plaques in non-stroke regions, $P = 0.048$ using Mann–Whitney test for independent samples, 6–7 fields from five mice (Fig. 4). These results demonstrate that plaque formation was significantly accelerated in ischaemic areas, but only transiently; a result that could explain why the middle cerebral artery occlusion study in mice led to an increase in the number of plaques 7 days later, whereas the human tissue analysis (where the timing of the stroke was unknown) did not show a difference. The increase in the amyloid burden was the result of the generation of new plaques, and not the growth of existing plaques in concordance with previous observations (Garcia-Alloza *et al*., 2006; Meyer-Luehmann *et al*., 2008).

The vessels targeted in these mice had small amounts of vascular amyloid deposition representing cerebral amyloid angiopathy (Masuda *et al*., 1988; Ellis *et al*., 1996). The presence of cerebral amyloid angiopathy insured that we were targeting arterioles (which are affected by cerebral amyloid angiopathy) rather than veins, and also allowed us to evaluate whether the rate of cerebral amyloid angiopathy progression (Robbins *et al*., 2006; Garcia-Alloza *et al*., 2009*a*) was affected by restricting blood flow. We found (Fig. 5) that cerebral amyloid angiopathy progression was accelerated nearly 2-fold in the occluded vessels (progression rate = 0.54% per day) compared with cerebral amyloid angiopathy affected vessels that were not targeted within the same mouse (progression rate 0.28% per day). While the trends suggest that the increased rate of progression of cerebral amyloid angiopathy is also transient (first week rate faster than the second week rate), our statistical model for cerebral amyloid angiopathy accumulation does not allow for comparison of slopes using only two time points so our analysis is limited to the overall rate of progression over both weeks.

β-amyloid production and degradation

We examined possible mechanisms for the rapid appearance of new plaques and cerebral amyloid angiopathy in the stroke volume. We postulated that the rapid appearance of new amyloid deposits could result from either an increase in β-amyloid production or a decrease in β-amyloid clearance. We used immunohistochemistry in brain sections from the mice with middle cerebral artery occlusion to probe for alterations in proteins in the stroke versus non-stroke area of the brain. We determined that the lesions did not alter the distribution or amount of presenilin 1 or BACE, which would reflect an increase in β-amyloid production. We were also unable to detect differences in the levels of

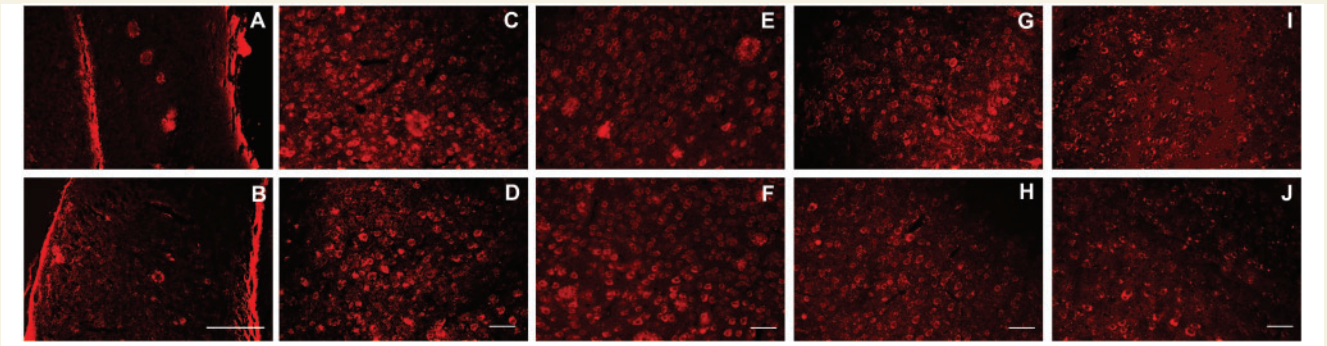

Figure 6 Transient middle cerebral artery occlusion did not affect proteins related to generation or degradation of β-amyloid. Representative examples of the limited effect of middle cerebral artery occlusion on proteins related to β-amyloid production or degradation using immunohistochemistry in post-mortem tissue sections. BACE, presenilin 1 and APP immunoreactivity was observed in the surrounding of senile plaques (not labelled), whereas neprilysin and insulin degrading enzyme signal was detected in neurons. No differences were observed in BACE (**A** and **B**), presenilin 1 (**C** and **D**), APP (**E** and **F**), neprilysin (**G** and **H**) or insulin degrading enzyme (**I** and **J**) (*top*: ipsilateral hemisphere; *bottom*: contralateral hemisphere). Scale bar = 200 μm.

neprilysin or insulin degrading enzyme, which would demonstrate a change in capacity for β-amyloid degradation. There were also no detectable differences in the levels of APP, arguing that an effect on the level of transgene expression was not responsible for the generation of new plaques (Fig. 6). The failure to find effects on factors related to either production or breakdown of β-amyloid suggests that the normal clearance pathways for β-amyloid along interstitial fluid drainage routes might be responsible for the increased β-amyloid deposition.

Discussion

In this report, we have demonstrated that ischaemic lesions in the brain led to rapid deposition of β-amyloid in two models of stroke and two transgenic mouse lines. Whereas previous studies showed correlations between cerebrovascular disease and β-amyloid deposition (Yow and Weller, 2002; Weller *et al*., 2008), our data suggest a direct causal link. Our transient middle cerebral artery occlusion studies are in accordance with previous studies where increased stroke volumes were observed in transgenic mice with Alzheimer's disease, when compared with wild-type mice (Zhang *et al*., 1997; Koistinaho *et al*., 2002), supporting the possibility of increased susceptibility to ischaemia as a result of neurotoxic effects of β-amyloid in the post-ischaemic brain (Zhang *et al*., 1997). Our middle cerebral artery occlusion studies showed a significant increase in senile plaque deposition as soon as 1 week after the procedure. We were not able to image the middle cerebral artery territory longitudinally in these mice, so we used an alternative model of stroke to follow the kinetics of this effect. We used intravital multiphoton microscopy and Rose bengal microstrokes to monitor the kinetics of the effect in real-time. We observed that the increased rate of amyloid deposition was transient. Newly deposited amyloid remained indefinitely, but the increased rate of deposition returned to the baseline level within 1 week. These surprising results demonstrate that stoppage of blood flow in the brain leads to rapid and robust deposition of fibrillar amyloid.

The transience of the effect of ischaemia on accelerated β-amyloid deposition might explain the observed absence of association between infarcted brain tissue and plaque deposition in post-mortem human tissue. Post-mortem studies in humans have generally not reported a tight association between cerebrovascular lesions and regions of extensive plaque and cerebral amyloid angiopathy formation, suggesting that cerebrovascular injury is at most just one of many contributors to β-amyloid deposition. This aspect is further blurred by the fact that many confounding factors may contribute including type 2 diabetes (Ott *et al*., 1999; Schrijvers *et al*., 2010), ApoE haplotype (Chartier-Harlin *et al*., 1994; Bickeboller *et al*., 1997) or previous pathologies. We examined a small number of cases, which does not represent an exhaustive evaluation that takes all these factors into consideration. Likewise, in our studies of human tissue with clinical diagnosis of both Alzheimer's disease and stroke, the strokes occurred well before patient death, making it very difficult to determine the precise timing of the events, since microstrokes are largely asymptomatic. A transient increase in amyloid deposition in the lesion area would be masked over time as the patient aged and amyloid deposition continued throughout the brain. Thus, our results in animal models confirm the majority of the clinical reports of the risk of Alzheimer's disease following stroke (Leys *et al*., 2005; Rastas *et al*., 2007; Helzner *et al*., 2009), and may explain the minority of reports where a risk of Alzheimer's disease was described if the interval between cerebral ischaemia and death was short. Even a transient increase in plaque deposition may nonetheless be relevant to an individual's risk of dementia and might thus contribute to the observed associations between vascular risk factors and dementia in humans (Elias *et al*., 1993; Breteler, 1994, 2000; Launer *et al*., 1995; Kalaria, 2000; Roher *et al*., 2003; Luchsinger and Mayeux, 2004; Honig *et al*., 2005). Vascular disease may also contribute to the inaccuracies in diagnosis of Alzheimer's disease, as an additional brain insult may exacerbate the cause or causes of the underlying dementia.

In clinical trials, for instance, cerebrovascular disease is now commonly used as an exclusion criterion (Dodge *et al.*, 2011; McKhann *et al.*, 2011).

While the mechanism of rapid amyloid deposition is unknown, it appears not to be related to changes in protein levels related to production (APP, presenilin 1 and BACE) or degradation (neprilysin and insulin degrading enzyme) of β-amyloid. Although we cannot exclude that alternative methods could detect differences in BACE, as previously shown in ischaemic Sprague-Dawley rats (Tesco *et al.*, 2007), the use of standard immunohistochemistry approaches to detect differences between the ischaemic and non-ischaemic areas in animals has been demonstrated to be effective (Wen *et al.*, 2004). These studies showed an increase in BACE levels after 24–48 h after middle cerebral artery occlusion in rats. We found no differences in BACE levels after 1 week, suggesting that if there is a modest increase in BACE levels acutely, that it resolves within a few days, as predicted in a model where an increase in the rate of β-amyloid deposition following ischaemia is transient. In certain hypoxia models, it has been shown that hypoxia facilitates APP processing by an upregulation of BACE1 gene transcription (Sun *et al.*, 2006) and that it may also facilitate β- and γ-cleavage (Li *et al.*, 2009). On the other hand, degradation enzymes have also been reported to mediate Alzheimer's disease progression. Insulin degrading enzyme has been shown to increase in a rat middle cerebral artery occlusion model (Hiltunen *et al.*, 2009) and reductions in neprilysin may increase β-amyloid formation (Iwata *et al.*, 2001). Moreover, it seems that neprilysin activity is independent of other β-amyloid degrading enzymes, such as endothelin-converting enzymes (Eckman *et al.*, 2006). Our data related to neprilysin levels are in accordance to the previous studies in a middle cerebral artery occlusion rat model (Hiltunen *et al.*, 2009), where no changes were observed in neprilysin levels up to 30 days after the procedure. A limitation of our study is that we examined protein levels and not activity of these enzymes. While generally correlated, it is possible that changes in activity can occur independently of total protein levels.

Likewise, as ischaemia is always accompanied by neuroinflammation, it is possible that a direct or indirect consequence of an immune response plays a role in amyloid deposition. However, in the absence of observable changes in the mediators of β-amyloid production or degradation, it is likely that locally impaired clearance results in the accumulation of amyloid deposits, although no specific experiments were carried out to test this explicitly. Our data are consistent with the model of reduced amyloid clearance along interstitial fluid drainage pathways (Yow and Weller, 2002; Weller *et al.*, 2008). According to this model, β-amyloid clearance depends on counter current drainage along arterioles. Pulsatile intravascular blood flow drives clearance in the perivascular space; when this is disrupted by vascular occlusion, there is a transient loss in clearance of soluble parenchymal materials. The reduced clearance leads to a high local concentration of β-amyloid, and this may facilitate aggregation. While this hypothesis is difficult to test *in vivo*, it remains the most likely candidate for the transient increase in β-amyloid deposition that is restricted to the volume affected by reduced blood flow. However, we cannot completely rule out the contribution of alternative mechanisms. As a note of caution, these experiments were performed in mouse models that overexpress mutant human APP, and it is possible that these models do not accurately reflect the human condition.

Although other studies have suggested a link between ischaemia and amyloid production (van Groen *et al.*, 2005; Makinen *et al.*, 2008), the current work is the first to demonstrate the deposition of β-amyloid as plaques and cerebral amyloid angiopathy in living animals. We used real-time imaging in living animals to show increased plaque deposition in areas local to the occluded arteriole, as well as an accelerated rate of progression of cerebral amyloid angiopathy in vessels that were already partially affected. An important additional implication of these results is the demonstration of an experimental approach to initiate plaque and cerebral amyloid angiopathy deposition *in vivo* in a precisely defined volume of the brain. This technique should allow discrimination of the molecular basis of seeding amyloid deposition, since plaques and cerebral amyloid angiopathy can be induced to form within a small spatial and temporal window.

Finally, identifying cerebrovascular lesions as even a partial contributor towards β-amyloid deposition would have potential implications for preventing or slowing the progression of Alzheimer's disease and cerebral amyloid angiopathy. Additionally, the increased susceptibility of the APP mouse brain to ischaemic insults suggests a feed-forward cycle where ischaemia and amyloid deposition exacerbate each other. Although many candidate approaches have been suggested for inhibiting the β-amyloid pathway (McLaurin *et al.*, 2000; Bacskai *et al.*, 2001; Townsend *et al.*, 2006; Prada *et al.*, 2007; Rajendran *et al.*, 2008; Bateman *et al.*, 2009; Elvang *et al.*, 2009; Garcia-Alloza *et al.*, 2009*b*) none has yet been shown to block progression of the human diseases. Vascular disease, conversely, has a large number of established treatments, and therefore further studies to assess this possibility might set the basis for future attempts to prevent dementia.

Funding

National Institutes of Health (EB00768 to B.J.B.); (AG021084, AG005134 to M.P.F.); (RYC-2008-02333; L'oreal-UNESCO 2010; PN I+D+I 2008–2011: ISCIII Subdirección General de Evaluación y Fomento de la Investigación PS09/00969 to M.G.-A.).

References

Bacskai BJ, Kajdasz ST, Christie RH, Carter C, Games D, Seubert P, et al. Imaging of amyloid-beta deposits in brains of living mice permits direct observation of clearance of plaques with immunotherapy. Nat Med 2001; 7: 369–72.

Bateman RJ, Siemers ER, Mawuenyega KG, Wen G, Browning KR, Sigurdson WC, et al. A gamma-secretase inhibitor decreases amyloid-beta production in the central nervous system. Ann Neurol 2009; 66: 48–54.

Bickeboller H, Campion D, Brice A, Amouyel P, Hannequin D, Didierjean O, et al. Apolipoprotein E and Alzheimer disease: genotype-specific risks by age and sex. Am J Hum Genet 1997; 60: 439–46.

Breteler MM. Vascular risk factors for Alzheimer's disease: an epidemiologic perspective. Neurobiol Aging 2000; 21: 153–60.

Breteler MM, Claus JJ, Grobbee DE, Hofman A. Cardiovascular disease and distribution of cognitive function in elderly people: the Rotterdam Study. Br Med J 1994; 308: 1604–8.

Chartier-Harlin MC, Parfitt M, Legrain S, Perez-Tur J, Brousseau T, Evans A, et al. Apolipoprotein E, epsilon 4 allele as a major risk factor for sporadic early and late-onset forms of Alzheimer's disease: analysis of the 19q13.2 chromosomal region. Hum Mol Genet 1994; 3: 569–74.

de Leeuw FE, de Groot JC, Oudkerk M, Witteman JC, Hofman A, van Gijn J, et al. Hypertension and cerebral white matter lesions in a prospective cohort study. Brain 2002; 125: 765–72.

Dodge HH, Chang CC, Kamboh IM, Ganguli M. Risk of Alzheimer's disease incidence attributable to vascular disease in the population. Alzheimers Dement 2011; 7: 356–60.

Eckman EA, Adams SK, Troendle FJ, Stodola BA, Kahn MA, Fauq AH, et al. Regulation of steady-state beta-amyloid levels in the brain by neprilysin and endothelin-converting enzyme but not angiotensin-converting enzyme. J Biol Chem 2006; 281: 30471–8.

Elias MF, Wolf PA, D'Agostino RB, Cobb J, White LR. Untreated blood pressure level is inversely related to cognitive functioning: the Framingham Study. Am J Epidemiol 1993; 138: 353–64.

Ellis RJ, Olichney JM, Thal LJ, Mirra SS, Morris JC, Beekly D, et al. Cerebral amyloid angiopathy in the brains of patients with Alzheimer's disease: the CERAD experience, Part XV. Neurology 1996; 46: 1592–6.

Elvang AB, Volbracht C, Pedersen LO, Jensen KG, Karlsson JJ, Larsen SA, et al. Differential effects of gamma-secretase and BACE1 inhibition on brain Abeta levels in vitro and in vivo. J Neurochem 2009; 110: 1377–87.

Garcia-Alloza M, Borrelli LA, Hyman BT, Bacskai BJ. Antioxidants have a rapid and long-lasting effect on neuritic abnormalities in APP:PS1 mice. Neurobiol Aging 2010; 31: 2058–68.

Garcia-Alloza M, Prada C, Lattarulo C, Fine S, Borrelli LA, Betensky R, et al. Matrix metalloproteinase inhibition reduces oxidative stress associated with cerebral amyloid angiopathy in vivo in transgenic mice. J Neurochem 2009a; 109: 1636–47.

Garcia-Alloza M, Robbins EM, Zhang-Nunes SX, Purcell SM, Betensky RA, Raju S, et al. Characterization of amyloid deposition in the APPswe/PS1dE9 mouse model of Alzheimer disease. Neurobiol Dis 2006; 24: 516–24.

Garcia-Alloza M, Subramanian M, Thyssen D, Borrelli LA, Fauq A, Das P, et al. Existing plaques and neuritic abnormalities in APP:PS1 mice are not affected by administration of the gamma-secretase inhibitor LY-411575. Mol Neurodegener 2009b; 4: 19.

Helzner EP, Luchsinger JA, Scarmeas N, Cosentino S, Brickman AM, Glymour MM, et al. Contribution of vascular risk factors to the progression in Alzheimer disease. Arch Neurol 2009; 66: 343–8.

Hiltunen M, Makinen P, Peraniemi S, Sivenius J, van Groen T, Soininen H, et al. Focal cerebral ischemia in rats alters APP processing and expression of Abeta peptide degrading enzymes in the thalamus. Neurobiol Dis 2009; 35: 103–13.

Hofman A, Ott A, Breteler MM, Bots ML, Slooter AJ, van Harskamp F, et al. Atherosclerosis, apolipoprotein E, and prevalence of dementia and Alzheimer's disease in the Rotterdam Study. Lancet 1997; 349: 151–4.

Honig LS, Kukull W, Mayeux R. Atherosclerosis and AD: analysis of data from the US National Alzheimer's Coordinating Center. Neurology 2005; 64: 494–500.

Hsiao K, Chapman P, Nilsen S, Eckman C, Harigaya Y, Younkin S, et al. Correlative memory deficits, Abeta elevation, and amyloid plaques in transgenic mice. Science 1996; 274: 99–102.

Hyman BT. The neuropathological diagnosis of Alzheimer's disease: clinical-pathological studies. Neurobiol Aging 1997; 18: S27–32.

Iwata N, Tsubuki S, Takaki Y, Shirotani K, Lu B, Gerard NP, et al. Metabolic regulation of brain Abeta by neprilysin. Science 2001; 292: 1550–2.

Jankowsky JL, Slunt HH, Ratovitski T, Jenkins NA, Copeland NG, Borchelt DR. Co-expression of multiple transgenes in mouse CNS: a comparison of strategies. Biomol Eng 2001; 17: 157–65.

Kalaria RN. The role of cerebral ischemia in Alzheimer's disease. Neurobiol Aging 2000; 21: 321–30.

Kivipelto M, Helkala EL, Laakso MP, Hanninen T, Hallikainen M, Alhainen K, et al. Apolipoprotein E epsilon4 allele, elevated midlife total cholesterol level, and high midlife systolic blood pressure are independent risk factors for late-life Alzheimer disease. Ann Intern Med 2002; 137: 149–55.

Koistinaho M, Kettunen MI, Goldsteins G, Keinanen R, Salminen A, Ort M, et al. Beta-amyloid precursor protein transgenic mice that harbor diffuse A beta deposits but do not form plaques show increased ischemic vulnerability: role of inflammation. Proc Natl Acad Sci USA 2002; 99: 1610–5.

Kuchibhotla KV, Goldman ST, Lattarulo CR, Wu HY, Hyman BT, Bacskai BJ. Abeta plaques lead to aberrant regulation of calcium homeostasis in vivo resulting in structural and functional disruption of neuronal networks. Neuron 2008; 59: 214–25.

Launer LJ, Masaki K, Petrovitch H, Foley D, Havlik RJ. The association between midlife blood pressure levels and late-life cognitive function. The Honolulu-Asia Aging Study. JAMA 1995; 274: 1846–51.

Launer LJ, Petrovitch H, Ross GW, Markesbery W, White LR. AD brain pathology: vascular origins? Results from the HAAS autopsy study. Neurobiol Aging 2008; 29: 1587–90.

Leys D, Henon H, Mackowiak-Cordoliani MA, Pasquier F. Poststroke dementia. Lancet Neurol 2005; 4: 752–9.

Li L, Zhang X, Yang D, Luo G, Chen S, Le W. Hypoxia increases Abeta generation by altering beta- and gamma-cleavage of APP. Neurobiol Aging 2009; 30: 1091–8.

Luchsinger JA, Mayeux R. Cardiovascular risk factors and Alzheimer's disease. Curr Atheroscler Rep 2004; 6: 261–6.

Luchsinger JA, Reitz C, Patel B, Tang MX, Manly JJ, Mayeux R. Relation of diabetes to mild cognitive impairment. Arch Neurol 2007; 64: 570–5.

Luchsinger JA, Tang MX, Shea S, Mayeux R. Hyperinsulinemia and risk of Alzheimer disease. Neurology 2004; 63: 1187–92.

Makinen S, van Groen T, Clarke J, Thornell A, Corbett D, Hiltunen M, et al. Coaccumulation of calcium and beta-amyloid in the thalamus after transient middle cerebral artery occlusion in rats. J Cereb Blood Flow Metab 2008; 28: 263–8.

Masuda J, Tanaka K, Ueda K, Omae T. Autopsy study of incidence and distribution of cerebral amyloid angiopathy in Hisayama, Japan. Stroke 1988; 19: 205–10.

McKhann GM, Knopman DS, Chertkow H, Hyman BT, Jack CR Jr, Kawas CH, et al. The diagnosis of dementia due to Alzheimer's disease: recommendations from the National Institute on Aging-Alzheimer's Association workgroups on diagnostic guidelines for Alzheimer's disease. Alzheimers Dement 2011; 7: 263–9.

McLaurin J, Golomb R, Jurewicz A, Antel JP, Fraser PE. Inositol stereoisomers stabilize an oligomeric aggregate of Alzheimer amyloid beta peptide and inhibit abeta -induced toxicity. J Biol Chem 2000; 275: 18495–502.

McLellan ME, Kajdasz ST, Hyman BT, Bacskai BJ. In vivo imaging of reactive oxygen species specifically associated with thioflavine S-positive amyloid plaques by multiphoton microscopy. J Neurosci 2003; 23: 2212–7.

Meyer-Luehmann M, Spires-Jones TL, Prada C, Garcia-Alloza M, de Calignon A, Rozkalne A, et al. Rapid appearance and local toxicity of amyloid-beta plaques in a mouse model of Alzheimer's disease. Nature 2008; 451: 720–4.

Ott A, Slooter AJ, Hofman A, van Harskamp F, Witteman JC, Van Broeckhoven C, et al. Smoking and risk of dementia and Alzheimer's disease in a population-based cohort study: the Rotterdam Study. Lancet 1998; 351: 1840–3.

Ott A, Stolk RP, van Harskamp F, Pols HA, Hofman A, Breteler MM. Diabetes mellitus and the risk of dementia: The Rotterdam Study. Neurology 1999; 53: 1937–42.

Pappolla MA, Bryant-Thomas TK, Herbert D, Pacheco J, Fabra Garcia M, Manjon M, et al. Mild hypercholesterolemia is an early risk factor for the development of Alzheimer amyloid pathology. Neurology 2003; 61: 199–205.

Prada CM, Garcia-Alloza M, Betensky RA, Zhang-Nunes SX, Greenberg SM, Bacskai BJ, et al. Antibody-mediated clearance of amyloid-beta peptide from cerebral amyloid angiopathy revealed by quantitative in vivo imaging. J Neurosci 2007; 27: 1973–80.

Rajendran L, Schneider A, Schlechtingen G, Weidlich S, Ries J, Braxmeier T, et al. Efficient inhibition of the Alzheimer's disease beta-secretase by membrane targeting. Science 2008; 320: 520–3.

Rastas S, Verkkoniemi A, Polvikoski T, Juva K, Niinisto L, Mattila K, et al. Atrial fibrillation, stroke, and cognition: a longitudinal population-based study of people aged 85 and older. Stroke 2007; 38: 1454–60.

Razay G, Vreugdenhil A, Wilcock G. The metabolic syndrome and Alzheimer disease. Arch Neurol 2007; 64: 93–6.

Reitz C, Tang MX, Manly J, Mayeux R, Luchsinger JA. Hypertension and the risk of mild cognitive impairment. Arch Neurol 2007; 64: 1734–40.

Robbins EM, Betensky RA, Domnitz SB, Purcell SM, Garcia-Alloza M, Greenberg C, et al. Kinetics of cerebral amyloid angiopathy progression in a transgenic mouse model of Alzheimer disease. J Neurosci 2006; 26: 365–71.

Roher AE, Esh C, Kokjohn TA, Kalback W, Luehrs DC, Seward JD, et al. Circle of willis atherosclerosis is a risk factor for sporadic Alzheimer's disease. Arterioscler Thromb Vasc Biol 2003; 23: 2055–62.

Schrijvers EM, Witteman JC, Sijbrands EJ, Hofman A, Koudstaal PJ, Breteler MM. Insulin metabolism and the risk of Alzheimer disease: the Rotterdam Study. Neurology 2010; 75: 1982–7.

Seshadri S, Beiser A, Selhub J, Jacques PF, Rosenberg IH, D'Agostino RB, et al. Plasma homocysteine as a risk factor for dementia and Alzheimer's disease. N Engl J Med 2002; 346: 476–83.

Shin HK, Nishimura M, Jones PB, Ay H, Boas DA, Moskowitz MA, et al. Mild induced hypertension improves blood flow and oxygen metabolism in transient focal cerebral ischemia. Stroke 2008; 39: 1548–55.

Stone J. What initiates the formation of senile plaques? The origin of Alzheimer-like dementias in capillary haemorrhages. Med Hypotheses 2008; 71: 347–59.

Sun X, He G, Qing H, Zhou W, Dobie F, Cai F, et al. Hypoxia facilitates Alzheimer's disease pathogenesis by up-regulating BACE1 gene expression. Proc Natl Acad Sci USA 2006; 103: 18727–32.

Tesco G, Koh YH, Kang EL, Cameron AN, Das S, Sena-Esteves M, et al. Depletion of GGA3 stabilizes BACE and enhances beta-secretase activity. Neuron 2007; 54: 721–37.

Townsend M, Cleary JP, Mehta T, Hofmeister J, Lesne S, O'Hare E, et al. Orally available compound prevents deficits in memory caused by the Alzheimer amyloid-beta oligomers. Ann Neurol 2006; 60: 668–76.

van Groen T, Puurunen K, Maki HM, Sivenius J, Jolkkonen J. Transformation of diffuse beta-amyloid precursor protein and beta-amyloid deposits to plaques in the thalamus after transient occlusion of the middle cerebral artery in rats. Stroke 2005; 36: 1551–6.

Weller RO, Subash M, Preston SD, Mazanti I, Carare RO. Perivascular drainage of amyloid-beta peptides from the brain and its failure in cerebral amyloid angiopathy and Alzheimer's disease. Brain Pathol 2008; 18: 253–66.

Wen Y, Onyewuchi O, Yang S, Liu R, Simpkins JW. Increased beta-secretase activity and expression in rats following transient cerebral ischemia. Brain Res 2004; 1009: 1–8.

Yow HY, Weller RO. A role for cerebrovascular disease in determining the pattern of beta-amyloid depositio nin Alzheimer's disease. Neuropathol Appl Neurobiol 2002; 28: 149.

Zhang F, Eckman C, Younkin S, Hsiao KK, Iadecola C. Increased susceptibility to ischemic brain damage in transgenic mice overexpressing the amyloid precursor protein. J Neurosci 1997; 17: 7655–61.

Zhang S, Murphy TH. Imaging the impact of cortical microcirculation on synaptic structure and sensory-evoked hemodynamic responses in vivo. PLoS Biol 2007; 5: e119.